International Journal of Computational Engineering Science
Vol. 5, No. 4 (2004) 833–861

Imperial College Press
www.icpress.co.uk

ON THE POISSON'S RATIO EFFECT ON MIXED-MODE STRESS INTENSITY FACTORS AND T-STRESS IN FUNCTIONALLY GRADED MATERIALS

GLAUCIO H. PAULINO* and JEONG-HO KIM†
Department of Civil and Environmental Engineering,
University of Illinois at Urbana-Champhaign,
Newmark Laboratory, 205 North Mathews Avenue,
Urbana, IL 61801, USA
**paulino@uiuc.edu*
†*jhkim@engr.uconn.edu*

Poisson's ratio is an important factor for fracture of functionally graded materials (FGMs). It may have significant influence on fracture parameters (e.g. stress intensity factors and T-stress) for a crack in FGMs under mixed-mode loading conditions, while its effect on such parameters is negligible in homogeneous materials. For instance, when tension load is applied in the direction parallel to material gradation, the fracture parameters may show significant influence on the Poisson's ratio. This paper uses a new formulation, so-called non-equilibrium formulation, of the interaction integral method. It also presents a few numerical examples where Poisson's ratio is assumed either constant or linearly varying function, and Young's modulus is assumed to be exponential or hyperbolic-tangent function.

Keywords: Functionally graded material (FGM); fracture mechanics; stress intensity factor (SIF); T-stress; interaction integral; finite element method (FEM); Poisson's ratio.

1. Introduction

Fracture behavior of isotropic functionally graded materials has been investigated by evaluating mixed-mode stress intensity factors (SIFs)[1–7] and T-stress[7–10] of a stationary crack. The above investigations show that variation of material properties, e.g. Young's modulus, has a significant influence on both SIFs and T-stress in FGMs. However, when tension load is applied in the direction parallel to material gradation (see Fig. 1(a)), the more compliant part of the material may show more contraction than the stiffer part. This behavior affects the near crack-tip fields characterized by SIFs and T-stress. Such behavior is not observed for the case where tension load is applied in the direction perpendicular to material gradation (see Fig. 1(b)). Therefore this paper investigates the effect of Poisson's ratio on both SIFs and T-stress for the former case (illustrated by Fig. 1(a)). These fracture parameters are determined by means of a new formulation of the interaction integral method, which is called non-equilibrium formulation.

This paper is organized as follows. Section 2 comments on related work. Section 3 presents auxiliary fields for SIFs and T-stress using the non-equilibrium formulation of

†Current address: Department of Civil and Environmental Engineering, University of Connecticut, 261 Glenbrook Rd., Storrs, CT 06269-2037, USA.

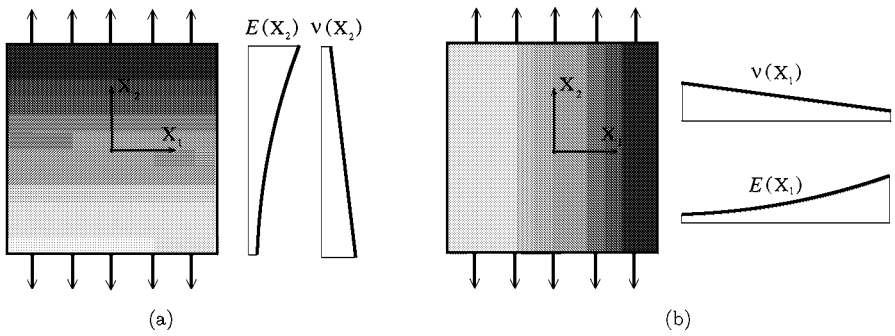

Fig. 1. Geometry and loading conditions: (a) load parallel to material gradation; (b) load perpendicular to material gradation.

the interaction integral (M-integral[a]) method. Section 4 explains the non-equilibrium formulation. Sections 5 and 6 establish the relationships between M and SIFs or T-stress, respectively. Sections 7 provides numerical aspects of the M-integral. Sections 8 presents numerical examples. Finally, Section 9 presents some conclusions of this work.

2. Related work

The interaction integral method is an accurate and robust scheme for evaluating mixed-mode stress intensity factors (SIFs) and T-stress. The method is formulated on the basis of conservation laws, which establish a conservation integral for two admissible states of an elastic solid: *actual* and *auxiliary*. Yau *et al.*[15] proposed the interaction integral method for evaluating SIFs in homogeneous isotropic materials. Recently, the interaction integral method has been investigated for fracture of FGMs and has been extended for evaluating SIFs[4,5,6,9] in isotropic FGMs. Dolbow and Gosz[4] employed the extended finite element method (X-FEM); Rao and Rahman[5] used the element-free Galerkin (EFG) method; and Kim and Paulino[6,9] used the finite element method (FEM). In addition, the method has also been used to evaluate T-stress (non-singular stress of the Williams's eigenfunction expansion[16]) in isotropic FGMs[9].

The finite element method (FEM) has been widely used for fracture analyses of FGMs. Eischen[1] has evaluated mixed-mode SIFs by means of the path-independent J_k^*-integral. Gu *et al.*[17] have evaluated SIFs using the standard J-integral. Anlas *et al.*[18] have calculated SIFs by means of the path-independent J_1^*-integral. Marur and Tippur[3] have investigated a crack normal to the material gradient by means of both the FEM and experiments. Bao and Cai[19] have studied delamination cracking in a graded ceramic/metal substrate under mechanical and thermal loads. Bao and Wang[20] have investigated periodic cracking in

[a]Here, the so-called M-integral should not be confused with the M-integral (conservation integral) of Knowles and Sternberg[11], Budiansky and Rice[12], and Chang and Chien[13]. Also, see the book by Kanninen and Popelar[14] for a review of conservation integrals in fracture mechanics.

graded ceramic/metal coatings under mechanical and thermal loads. Kim and Paulino[2] have evaluated mixed-mode SIFs by means of the path-independent J_k^*-integral, the modified crack closure (MCC), and the displacement correlation technique (DCT). The T-stress has also been computed by means of the FEM. Becker *et al.*[8] studied T-stress and finite crack kinking in FGMs. Recently, Kim and Paulino[9] used a unified approach of the interaction integral method for evaluating SIFs and T-stress in FGMs, and also investigated the effect of T-stress on crack initiation angles. Due to its generality, the FEM is the method of choice in this work.

3. Auxiliary fields

The interaction integral makes use of auxiliary fields, such as displacements ($\boldsymbol{u}^{aux}$), strains ($\boldsymbol{\varepsilon}^{aux}$), and stresses ($\boldsymbol{\sigma}^{aux}$). These auxiliary fields need to be suitably defined in order to evaluate mixed-mode SIFs and T-stress. There are various choices for the auxiliary fields. Here we adopt fields originally developed for homogeneous materials and use a "non-equilibrium formulation" which accounts for non-equilibrium due to the material mismatch between the homogeneous and graded materials. The auxiliary fields chosen in this paper are described below.

3.1. Displacement and strain fields for SIFs

For evaluating mixed-mode SIFs, we select the auxiliary displacement and strain fields as the Williams's[16] crack-tip asymptotic fields with the material properties sampled at the crack-tip location[1,21]. Fig. 2(a) shows a crack in an FGM under two-dimensional fields in local Cartesian and polar coordinates originating at the crack tip. The auxiliary displacement and strain fields are chosen as[16]:

$$u_i^{aux} = \frac{K_I^{aux}}{\mu^{\text{tip}}}\sqrt{\frac{r}{2\pi}}g_i^I(\theta) + \frac{K_{II}^{aux}}{\mu^{\text{tip}}}\sqrt{\frac{r}{2\pi}}g_i^{II}(\theta), \tag{1}$$

$$\varepsilon_{ij}^{aux} = \frac{1}{2}\left(u_{i,j}^{aux} + u_{j,i}^{aux}\right) \quad (i,j=1,2), \tag{2}$$

where μ^{tip} is the shear modulus at the crack tip, and K_I^{aux} and K_{II}^{aux} are the auxiliary mode I and mode II SIFs, respectively, and the angular functions $g_i(\theta)$ are given in many references, e.g. the paper by Eftis *et al.*[22].

3.2. Displacement and strain fields for T-stress

For evaluating T-stress, we choose the auxiliary displacement fields as those due to a point force in the x_1 direction, applied to the tip of a semi-infinite crack in an infinite *homogeneous* body as shown in Fig. 2(b). The auxiliary displacements and strains are obtained according

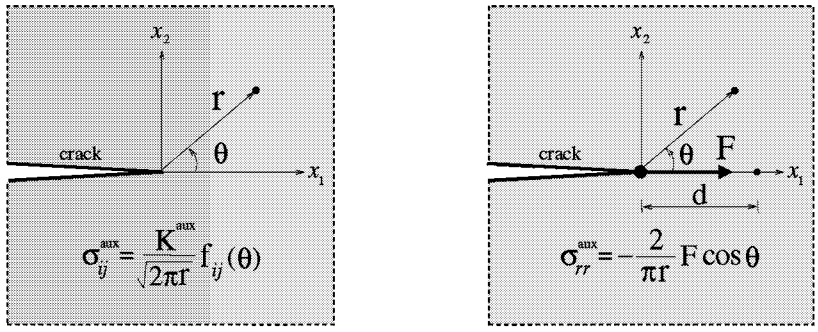

Fig. 2. Auxiliary fields for homogeneous materials: (a) Williams's solution[16] is used for SIF evaluation; (b) Michell's solution (see the book by Timoshenko and Goodier[23]) is used for T-stress evaluation.

to Michell's solution[23]:

$$\left\{ \begin{array}{c} u_1^{aux} \\ \\ u_2^{aux} \end{array} \right\} = \left\{ \begin{array}{l} -\frac{F(1+\kappa^{\rm tip})}{8\pi\mu^{\rm tip}} \ln\frac{r}{d} - \frac{F}{4\pi\mu^{\rm tip}} \sin^2\theta \\ \\ -\frac{F(\kappa^{\rm tip}-1)}{8\pi\mu^{\rm tip}}\theta + \frac{F}{4\pi\mu^{\rm tip}} \sin\theta\cos\theta \end{array} \right\} \tag{3}$$

$$\varepsilon_{ij}^{aux} = \frac{1}{2}\left(u_{i,j}^{aux} + u_{j,i}^{aux}\right) \quad (i,j=1,2), \tag{4}$$

where F is the point force applied at the crack tip, d is the coordinate of a fixed point on the x_1 axis (see Fig. 2(b)), $\mu^{\rm tip}$ is the shear modulus at the crack tip, and

$$\kappa^{\rm tip} = \begin{cases} (3-\nu_{\rm tip})/(1+\nu_{\rm tip}) & \text{for plane stress} \\ (3-4\nu_{\rm tip}) & \text{for plane strain.} \end{cases} \tag{5}$$

3.3. Stress fields for the non-equilibrium formulation

In the non-equilibrium formulation, the auxiliary stress fields are chosen as (see Fig. 3):

$$\sigma_{ij}^{aux} = C_{ijkl}(\boldsymbol{x})\ \varepsilon_{kl}^{aux}, \tag{6}$$

which differs from

$$\sigma_{ij}^{aux} = (C_{ijkl})_{\rm tip}\ \varepsilon_{kl}^{aux}, \tag{7}$$

where $C_{ijkl}(\boldsymbol{x})$ is the constitutive tensor of the actual FGM and $(C_{ijkl})_{\rm tip}$ is the constitutive tensor at the crack tip, as shown in Fig. 3. The derivatives of the auxiliary stress field are given by

$$\begin{aligned} \sigma_{ij,j}^{aux} &= C_{ijkl,j}(\boldsymbol{x})\ \varepsilon_{kl}^{aux} + C_{ijkl}(\boldsymbol{x})\ \varepsilon_{kl,j}^{aux} \\ &= \underline{(C_{ijkl})_{\rm tip}\ \varepsilon_{kl,j}^{aux}} + C_{ijkl,j}(\boldsymbol{x})\ \varepsilon_{kl}^{aux} + (C_{ijkl}(\boldsymbol{x}) - (C_{ijkl})_{\rm tip})\ \varepsilon_{kl,j}^{aux}, \end{aligned} \tag{8}$$

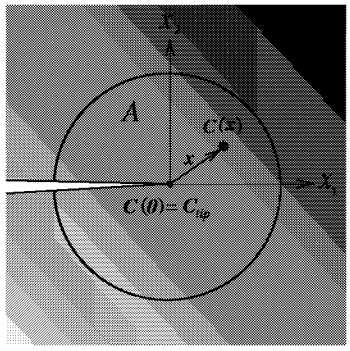

Fig. 3. Illustration of the interaction integral formulation considering material nonhomogeneity. Notice that $\boldsymbol{C}(\boldsymbol{x}) \neq \boldsymbol{C}_{tip}$ for $\boldsymbol{x} \neq \boldsymbol{0}$. The area A denotes a representative region around the crack tip.

where the underlined term in Eq.(8) vanishes. Thus the auxiliary stress fields selected in this formulation (see Eq.(6)) do not satisfy equilibrium, i.e. $\sigma^{aux}_{ij,j} \neq 0$ (no body forces or inertia). This choice of the auxiliary fields has been discussed by Dolbow and Gosz[4], but the interaction-integral formulation was not provided in their paper. This non-equilibrium in the stress field is considered in the M-integral formulation, which is discussed in detail below.

4. M-integral: Non-equilibrium formulation

The interaction integral is derived from the path-independent J-integral[24] for two admissible states of a cracked elastic FGM body. For the sake of numerical efficiency, the contour integral is transformed into an equivalent domain integral (EDI)[25]. The standard J-integral[24] is given by

$$J = \lim_{\Gamma_s \to 0} \int_{\Gamma_s} (\mathcal{W}\delta_{1j} - \sigma_{ij}\, u_{i,1})\, n_j\, d\Gamma, \tag{9}$$

where $\mathcal{W}$ is the strain energy density expressed by

$$\mathcal{W} = \frac{1}{2}\sigma_{ij}\varepsilon_{ij} = \frac{1}{2}\, C_{ijkl}\varepsilon_{kl}\varepsilon_{ij}, \tag{10}$$

and n_j is the outward normal vector to the contour Γ_s, as shown in Fig. 4.

Applying the divergence theorem and considering that the weight function q varies from unity at the crack tip to zero on Γ_0, as shown in Fig. 5, the equivalent domain integral (EDI) is obtained as:

$$J = \int_A (\sigma_{ij}\, u_{i,1} - \mathcal{W}\delta_{1j})\, q_{,j}\, dA + \int_A (\sigma_{ij}\, u_{i,1} - \mathcal{W}\delta_{1j})_{,j}\, q\, dA. \tag{11}$$

The J-integral of the superimposed fields (actual and auxiliary fields) is given by

$$J^s = J + J^{aux} + M \tag{12}$$

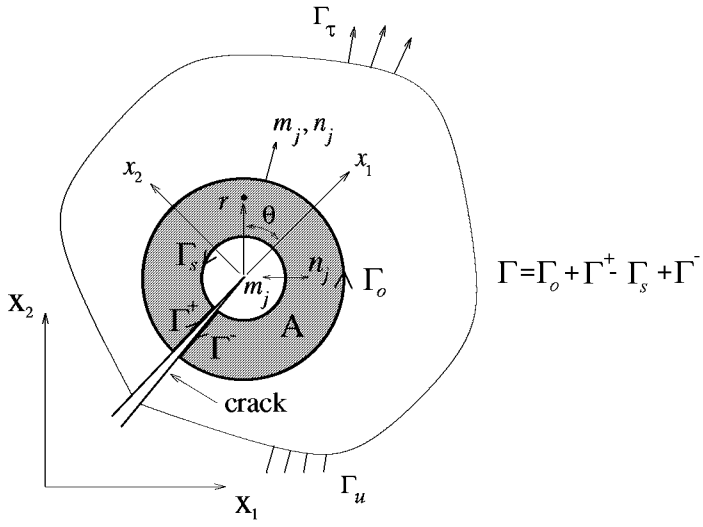

Fig. 4. Conversion of the contour integral into an equivalent domain integral (EDI) where $\Gamma = \Gamma_o + \Gamma^+ - \Gamma_s + \Gamma^-$, $m_j = n_j$ on Γ_o and $m_j = -n_j$ on Γ_s.

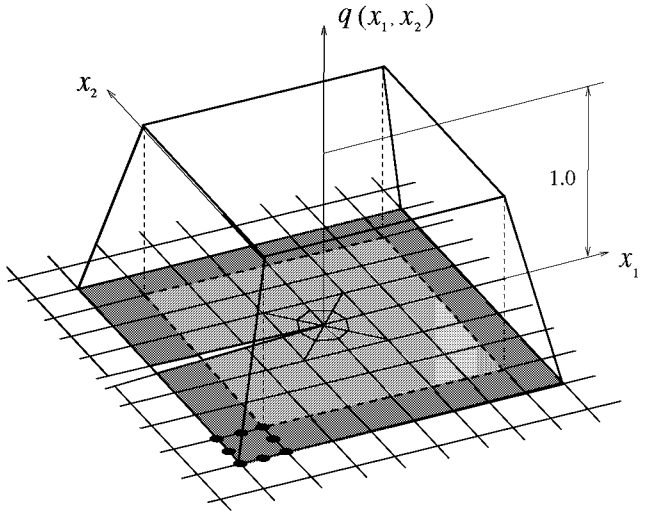

Fig. 5. Plateau weight function (q-function).

where J is given by Eq.(11), J^{aux} is given by

$$J^{aux} = \int_A (\sigma_{ij}^{aux}\ u_{i,1}^{aux} - \mathcal{W}^{aux}\delta_{1j})\ q_{,j}\ dA + \int_A \left\{\sigma_{ij}^{aux}\ u_{i,1}^{aux} - \frac{1}{2}\sigma_{ik}^{aux}\varepsilon_{ik}^{aux}\delta_{1j}\right\}_{,j} q\ dA,$$

and the resulting interaction integral (M) is given by

$$\begin{aligned} M = &\int_A \left\{\sigma_{ij}u_{i,1}^{aux} + \sigma_{ij}^{aux}u_{i,1} - \frac{1}{2}(\sigma_{ik}\varepsilon_{ik}^{aux} + \sigma_{ik}^{aux}\varepsilon_{ik})\delta_{1j}\right\} q_{,j}dA \\ &+ \int_A \left\{\sigma_{ij}u_{i,1}^{aux} + \sigma_{ij}^{aux}u_{i,1} - \frac{1}{2}(\sigma_{ik}\varepsilon_{ik}^{aux} + \sigma_{ik}^{aux}\varepsilon_{ik})\delta_{1j}\right\}_{,j} q\ dA. \end{aligned} \tag{13}$$

This derivation is now specialized in the context of the non-equilibrium formulation. Using the equality

$$\sigma_{ij}\varepsilon_{ij}^{aux} = \sigma_{ij}^{aux}\varepsilon_{ij}, \tag{14}$$

one rewrites Eq.(13) as

$$\begin{aligned} M = M_1 + M_2 = &\int_A \left\{\sigma_{ij}u_{i,1}^{aux} + \sigma_{ij}^{aux}u_{i,1} - \sigma_{ik}\varepsilon_{ik}^{aux}\delta_{1j}\right\} q_{,j}dA \\ &+ \int_A \left\{\sigma_{ij}u_{i,1}^{aux} + \sigma_{ij}^{aux}u_{i,1} - \sigma_{ik}\varepsilon_{ik}^{aux}\delta_{1j}\right\}_{,j} q\ dA. \end{aligned} \tag{15}$$

Moreover, the last term of the second integral (M_2) in Eq.(15) is expressed as

$$\begin{aligned} (\sigma_{ik}\varepsilon_{ik}^{aux}\delta_{1j})_{,j} &= (\sigma_{ik}\varepsilon_{ik}^{aux})_{,1} = (\sigma_{ij}\varepsilon_{ij}^{aux})_{,1} = (C_{ijkl}\varepsilon_{kl}\varepsilon_{ij}^{aux})_{,1} \\ &= C_{ijkl,1}\varepsilon_{kl}\varepsilon_{ij}^{aux} + C_{ijkl}\varepsilon_{kl,1}\varepsilon_{ij}^{aux} + C_{ijkl}\varepsilon_{kl}\varepsilon_{ij,1}^{aux} \\ &= C_{ijkl,1}\varepsilon_{kl}\varepsilon_{ij}^{aux} + \sigma_{ij}^{aux}\varepsilon_{ij,1} + \sigma_{ij}\varepsilon_{ij,1}^{aux}. \end{aligned} \tag{16}$$

Substitution of Eq.(16) into Eq.(15), and consideration of compatibility (actual and auxiliary) and equilibrium (actual) (i.e. $\sigma_{ij,j} = 0$ with no body force) lead to the following resulting interaction integral (M)

$$\begin{aligned} M = &\int_A \left\{\sigma_{ij}u_{i,1}^{aux} + \sigma_{ij}^{aux}u_{i,1} - \sigma_{ik}\varepsilon_{ik}^{aux}\delta_{1j}\right\} q_{,j}dA \\ &+ \int_A \left\{\underline{\sigma_{ij,j}^{aux}u_{i,1}} - C_{ijkl,1}\varepsilon_{kl}\varepsilon_{ij}^{aux}\right\} q\ dA, \end{aligned} \tag{17}$$

where the underlined term, which is the non-equilibrium term, appears due to non-equilibrium of the auxiliary stress fields (see Section 3.3).

5. Extraction of stress intensity factors

The relationship among J-integral and the mode I and mode II stress intensity factors is established as:

$$J_{\text{local}} = \frac{K_I^2 + K_{II}^2}{E_{\text{tip}}^*} \tag{18}$$

where

$$E^*_{\text{tip}} = \begin{cases} E_{\text{tip}} & \text{plane stress} \\ E_{\text{tip}}/(1-\nu^2_{\text{tip}}) & \text{plane strain} \end{cases} \tag{19}$$

By superimposing the actual and auxiliary fields, and using Eq.(18), one obtains

$$J^s_{\text{local}} = \frac{(K_I + K_I^{aux})^2 + (K_{II} + K_{II}^{aux})^2}{E^*_{\text{tip}}} \tag{20}$$

$$= J^{aux}_{\text{local}} + J_{\text{local}} + M_{\text{local}} \tag{21}$$

where

$$J^{aux}_{\text{local}} = \frac{(K_I^{aux})^2 + (K_{II}^{aux})^2}{E^*_{\text{tip}}} \tag{22}$$

and

$$M_{\text{local}} = \frac{2}{E^*_{\text{tip}}}(K_I K_I^{aux} + K_{II} K_{II}^{aux}). \tag{23}$$

The mode I stress intensity factor (K_I) can be computed by setting $K_I^{aux} = 1.0$ and $K_{II}^{aux} = 0.0$, i.e.

$$K_I = \frac{E^*_{\text{tip}}}{2} M^{(1)}_{\text{local}}. \tag{24}$$

Similarly, the mode II stress intensity factor (K_{II}) can be obtained by setting $K_I^{aux} = 0.0$ and $K_{II}^{aux} = 1.0$, i.e.

$$K_{II} = \frac{E^*_{\text{tip}}}{2} M^{(2)}_{\text{local}}. \tag{25}$$

The relationships (24) and (25) are essentially the same as those by Yau *et al.*[15], except that, for the FGM case, the material properties are evaluated at the crack-tip location.

6. Extraction of T-stress

The T-stress can be extracted from the interaction integral by nullifying the contributions of both singular (i.e. $O(r^{-1/2})$) and higher-order (i.e. $O(r^{1/2})$ and higher) terms. The M-integral in the form of line integral is obtained as (cf. Eq.(17))[9,10]

$$M_{\text{local}} = \lim_{\Gamma_s \to 0} \int_{\Gamma_s} \left\{ \sigma_{ik} \varepsilon^{aux}_{ik} \delta_{1j} - \sigma_{ij} u^{aux}_{i,1} - \sigma^{aux}_{ij} u_{i,1} \right\} n_j \, d\Gamma. \tag{26}$$

Here we can consider only the stress parallel to the crack direction, i.e.

$$\sigma_{ij} = T \delta_{1i} \delta_{1j}. \tag{27}$$

Using the stress-strain and strain-displacement relationships for the actual fields, one obtains

$$u_{1,1} = \varepsilon_{11} = \frac{1+\kappa(\boldsymbol{x})}{8\mu(\boldsymbol{x})} T, \quad u_{2,2} = \varepsilon_{22} = \frac{\kappa(\boldsymbol{x})-3}{8\mu(\boldsymbol{x})} T, \quad u_{1,2} + u_{2,1} = 0. \tag{28}$$

Substituting Eqs.(27) and (28) into Eq.(26), one obtains

$$M_{\text{local}} = -\lim_{\Gamma_s \to 0} \int_{\Gamma_s} \sigma_{ij}^{aux} n_j u_{i,1} \, d\Gamma = -\frac{T}{E^*_{\text{tip}}} \lim_{\Gamma_s \to 0} \int_{\Gamma_s} \sigma_{ij}^{aux} n_j \, d\Gamma. \tag{29}$$

Because the force F is in equilibrium (see Fig. 2(b))

$$F = -\lim_{\Gamma_s \to 0} \int_{\Gamma_s} \sigma_{ij}^{aux} n_j \, d\Gamma, \tag{30}$$

and thus the following relationship is readily obtained

$$T = \frac{E^*_{\text{tip}}}{F} M_{\text{local}}. \tag{31}$$

where E^*_{tip} is given by Eq.(19).

7. Numerical aspects

For numerical computation by means of the FEM, the M-integral is evaluated first in the global coordinates (M_{global}) and then transformed to the local coordinates (M_{local}). Thus the global interaction integral $(M_m)_{\text{global}}$ is obtained as $(m = 1, 2)$:

$$\begin{aligned}(M_m)_{\text{global}} = &\int_A \left\{ \sigma_{ij} u_{i,m}^{aux} + \sigma_{ij}^{aux} u_{i,m} - \sigma_{ik} \varepsilon_{ik}^{aux} \delta_{mj} \right\} \frac{\partial q}{\partial X_j} \, dA \\ &+ \int_A \left\{ \underline{\sigma_{ij,j}^{aux} u_{i,m}} - C_{ijkl,m} \varepsilon_{ij} \varepsilon_{kl}^{aux} \right\} q \, dA,\end{aligned} \tag{32}$$

where (X_1, X_2) are the global coordinates shown in Fig. 4, and the derivatives of the auxiliary strain fields $\sigma_{ij,j}^{aux}$ must be carefully evaluated as discussed below. The following transformation $(i, j = 1, 2)$

$$(M_i)_{\text{local}} = \alpha_{ij}(\theta)(M_i)_{\text{global}}, \quad \alpha_{ij}(\theta) = \begin{bmatrix} \cos\theta & \sin\theta \\ -\sin\theta & \cos\theta \end{bmatrix}, \tag{33}$$

allows one to calculate M_{local} as

$$M_{\text{local}} = (M_1)_{\text{local}} = (M_1)_{\text{global}} \cos\theta + (M_2)_{\text{global}} \sin\theta. \tag{34}$$

For the sake of generality, in this paper we determine derivatives of material properties by using shape function derivatives of finite elements[2,26]. The derivatives of the auxiliary stress field are obtained as:

$$\sigma_{ij,j}^{aux} = C_{ijkl,j} \, \varepsilon_{kl}^{aux} + C_{ijkl} \, \varepsilon_{kl,j}^{aux}. \tag{35}$$

A simple and accurate approach consists of evaluating the derivatives of the $\boldsymbol{C}$ tensor (see Eqs.(32) and (35)) by using shape function derivatives. The derivatives of a generic material quantity P (e.g. C_{ijkl}) are obtained as

$$\frac{\partial P}{\partial X_m} = \sum_{i=1}^{n} \frac{\partial N_i}{\partial X_m} P_i, \quad (m = 1, 2), \tag{36}$$

where n is the number of element nodes and $N_i = N_i(\xi, \eta)$ are the shape functions which can be found in many references, e.g.[27]. The derivatives $\partial N_i/\partial X_m$ are obtained as

$$\begin{Bmatrix} \partial N_i/\partial X_1 \\ \\ \partial N_i/\partial X_2 \end{Bmatrix} = \boldsymbol{J}^{-1} \begin{Bmatrix} \partial N_i/\partial \xi \\ \\ \partial N_i/\partial \eta \end{Bmatrix} \tag{37}$$

where $\boldsymbol{J}^{-1}$ is the inverse of the standard Jacobian matrix relating (X_1, X_2) with (ξ, η), i.e.

$$\boldsymbol{J} = \begin{bmatrix} \partial X_1/\partial \xi & \partial X_2/\partial \xi \\ \\ \partial X_1/\partial \eta & \partial X_2/\partial \eta \end{bmatrix}. \tag{38}$$

8. Numerical examples

The Poisson's ratio effect on SIFs and T-stress is investigated by means of the non-equilibrium formulation of the interaction integral method in the following examples:

(**1**) Verification example: Inclined center crack

(**2**) Center crack in an exponentially graded plate

(**3**) Center crack in a composite plate

The examples are analyzed using the FEM code I-FRANC2D[b] (Illinois - FRacture ANalysis Code 2D), which is based on the code FRANC2D[28,29] developed at Cornell University. The I-FRANC2D special-purpose code has specific techniques to evaluate mixed-mode SIFs and T-stress in FGMs including the interaction integral method. The I-FRANC2D element library for FGMs consists of *graded elements*[2,26,30], which incorporate the material gradient at the size-scale of the element. The specific graded elements used here are based on the *generalized isoparametric formulation* presented by Kim and Paulino[2], who have also compared the performance of these elements with that of conventional homogeneous elements (produces a step-wise constant approximation to a continuous material property field)[26].

All the geometry is discretized with isoparametric graded elements[2]. The specific elements used consist of singular quarter-point six-node triangles (T6qp) for crack-tip discretization, eight-node serendipity elements (Q8) for a circular region surrounding the crack-tip elements, and regular six-node triangles (T6) in a transition zone between regions of Q8 elements (see, for example, Fig. 7).

For verification of the present numerical scheme, the first example is investigated, which has available semi-analytical solutions provided by Konda and Ergogan[39]. Afterwards, in order to show the effect of Poisson's ratio on SIFs and T-stress, two more examples are considered where there is a center crack in a plate subjected to tension load applied parallel to the direction of material gradation. The first example investigates exponential

[b]The FEM code I-FRANC2D was formerly called FGM-FRANC2D[2].

variation for Young's modulus, and the second one considers hyperbolic-tangent variation. Exponentially graded materials have been extensively studied for fracture of FGMs in the literature[1,2,4,5,18,26,30–40]. A hyperbolic-tangent function is convenient to model material properties over a wide range from smooth transition to abrupt transition[6–9] (e.g. "bimaterial interfaces").

8.1. Verification example: Inclined center crack

This example serves as a verification example in the present numerical scheme. Konda and Erdogan [39] have investigated the mixed-mode crack problem in an unbounded nonhomogeneous elastic medium considering plane state conditions. The crack is arbitrarily oriented with respect to the material property gradient. This problem is solved here by means of the FEM by considering a plate that is large relative to the crack size ($a/W = 0.1$), as illustrated by Figure 6(a), which shows an interior inclined crack of length $2a$ with angle θ in a finite two-dimensional plate, Figure 6(b) shows a complete mesh configuration, and Figure 6(c) shows a mesh detail using 12 sectors (S12) and 4 rings (R4) around the crack tip. The applied load corresponds to $\sigma_{22}(X_1, 10) = \varepsilon_0 E_0 e^{\beta X_1}$. The displacement boundary condition is prescribed such that $u_2 = 0$ along the lower edge and $u_1 = 0$ for the node at the left hand side. This loading results in a uniform strain $\varepsilon_{22}(X_1, X_2) = \varepsilon_0$ in a corresponding uncracked structure.

Young's modulus is an exponential function of X_1 given by

$$E(X_1) = E_0\ e^{\beta X_1},$$

where the nonhomogeneity parameter β is given by

$$\beta = \frac{1}{2W} \log\left[\frac{E(W)}{E(-W)}\right], \tag{39}$$

which has units $[length]^{-1}$. The Poisson's ratio is constant. The typical mesh discretization consists of 1565 Q8, 173 T6, and 24 T6qp elements, with a total of 1762 elements and 5344 nodes. The following data were used for the FEM analysis:

$$\begin{gathered} a/W = 0.1,\ L/W = 1 \\ \beta a = 0.5,\ \varepsilon_0 = 1.0,\ E_0 = 1 \\ \theta = 0^\circ \text{ to } 90^\circ \\ \text{plane stress and } 2 \times 2 \text{ Gauss quadrature.} \end{gathered} \tag{40}$$

Table 1 compares the present FEM results for normalized SIFs obtained by the non-equilibrium formulation of the M-integral with semi-analytical solutions provided by Konda and Erdogan[39] for various geometric angles of a crack in FGMs. Notice that the present results for normalized SIFs are in excellent agreement with those by Konda and Erdogan[39].

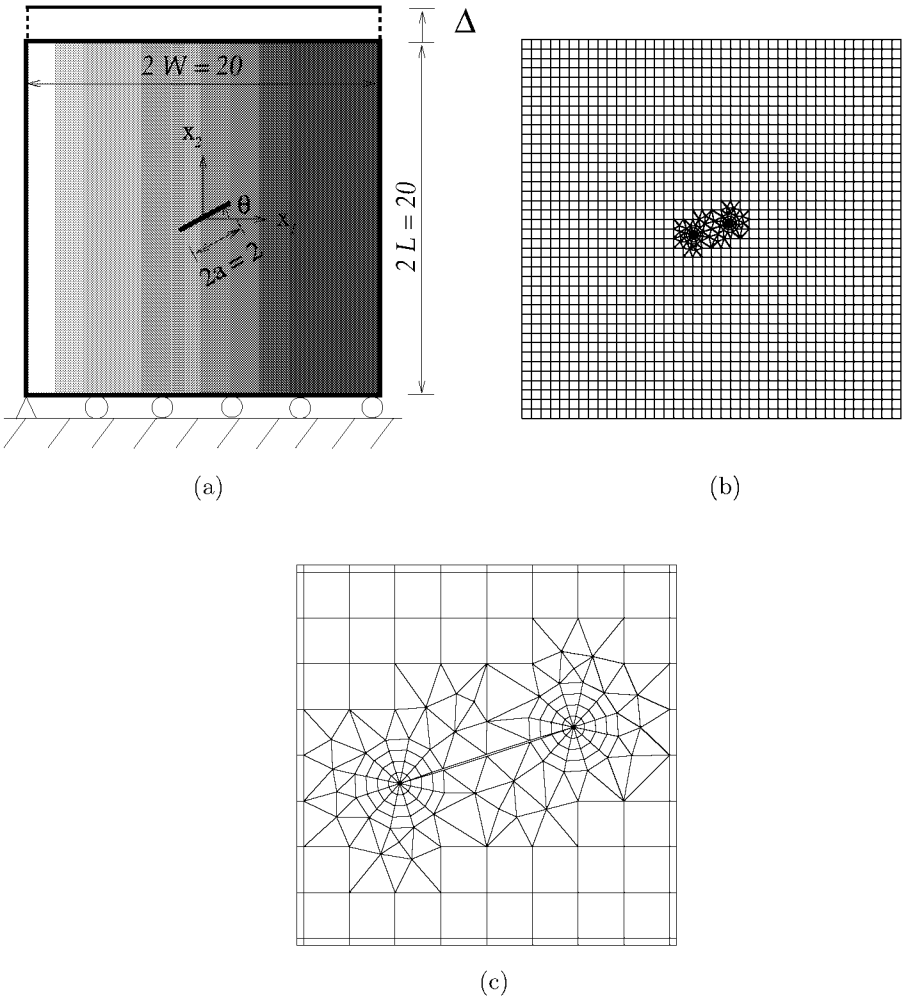

Fig. 6. Example 1: FGM plate with an inclined crack with geometric angle θ: (a) geometry and BCs under fixed-grip loading; (b) typical finite element mesh; (c) mesh detail using 12 sectors (S12) and 4 rings (R4) around the crack tips ($\theta = 18°$ counter-clockwise).

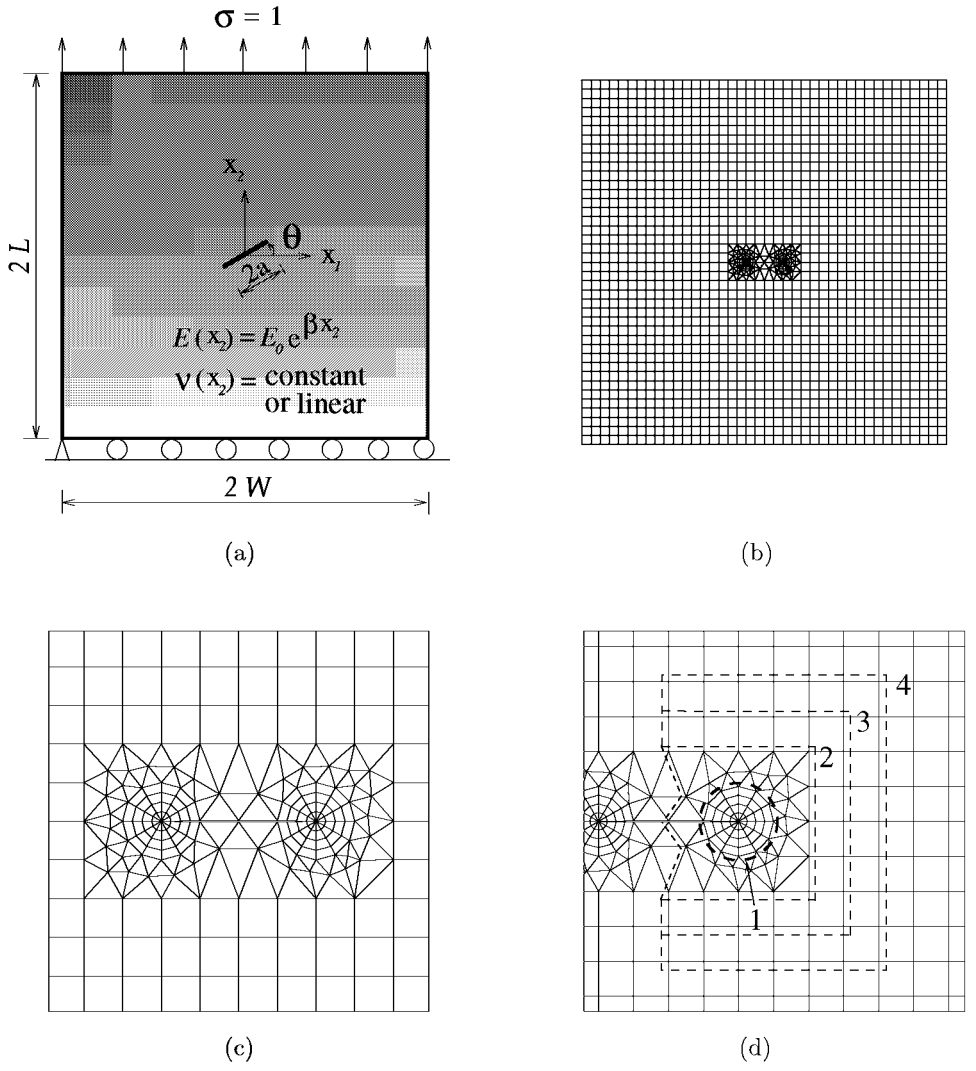

Fig. 7. Example 2: FGM plate with an inclined center crack. (a) geometry and BCs; (b) complete finite element mesh ($\theta = 0°$); (c) mesh detail using 12 sectors (S12) and 4 rings (R4) of elements around the crack tip; (d) contours used for EDI computation.

Table 1. Example 1: comparison of normalized mixed-mode SIFs in FGMs for βa=0.5 ($K_0 = \varepsilon_0 E_0 \sqrt{\pi a}$) (see Figure 6).

Method	θ	K_I^+/K_0	K_{II}^+/K_0	K_I^-/K_0	K_{II}^-/K_0
Konda & Erdogan[39]	0°	1.424	0.000	0.674	0.000
	18°	1.285	0.344	0.617	0.213
	36°	0.925	0.548	0.460	0.365
	54°	0.490	0.532	0.247	0.397
	72°	0.146	0.314	0.059	0.269
	90°	0.000	0.000	0.000	0.000
Present	0°	1.4234	0.0000	0.6657	0.0000
	18°	1.2835	0.3454	0.6104	0.2112
	36°	0.9224	0.5502	0.4559	0.3625
	54°	0.4880	0.5338	0.2451	0.3943
	72°	0.1451	0.3147	0.0587	0.2670
	90°	0.0000	0.0000	0.0000	0.0000

8.2. Center crack in an exponentially graded plate

This example investigates a center crack in an exponentially graded plate under tension loading applied parallel to the direction of material gradation (see Fig. 1(a)). Fig. 7(a) shows a center crack of length $2a$ located in a finite two-dimensional FGM plate under constant remote tension, Fig. 7(b) shows the complete mesh configuration, Fig. 7(c) shows the mesh detail using 12 sectors (S12) and 4 rings (R4) around the crack tips, and Fig. 7(d) shows four contours used for EDI computation. The applied load corresponds to $\sigma_{22}(X_1, L) = \sigma = 1.0$. The displacement boundary conditions (BCs) are prescribed such that $u_1 = 0$ and $u_2 = 0$ at the left-corner node of the bottom edge and $u_2 = 0$ for the nodes of the bottom edge. The mesh discretization consists of 1639 Q8, 124 T6, and 24 T6qp elements, with a total of 1787 elements and 5392 nodes.

Young's modulus is an exponential function of X_2 given by

$$E(X_2) = E_0 \, e^{\beta X_2},$$

where the nonhomogeneity parameter β is given by

$$\beta = \frac{1}{2L} \log \left[\frac{E(L)}{E(-L)} \right], \tag{41}$$

which has units $[length]^{-1}$. The Poisson's ratio is taken as follows:

- Constant Poisson's ratio, $\nu(X_2)$= 0.1, 0.2, 0.3,0.4,0.45
- Linearly varying Poisson's ratio, $\nu(X_2)$= (0.2, 0.3,0.4,0.45) $\rightarrow$ 0.1

The following data were used for the FEM analysis:

$$\begin{gathered} a/W = 0.08 \text{ to } 0.5, \;\; L/W = 1 \\ \beta a = (0.0 \text{ to } 0.5), \;\; E_0 = 1 \\ \text{plane stress and } 2 \times 2 \text{ Gauss quadrature.} \end{gathered} \tag{42}$$

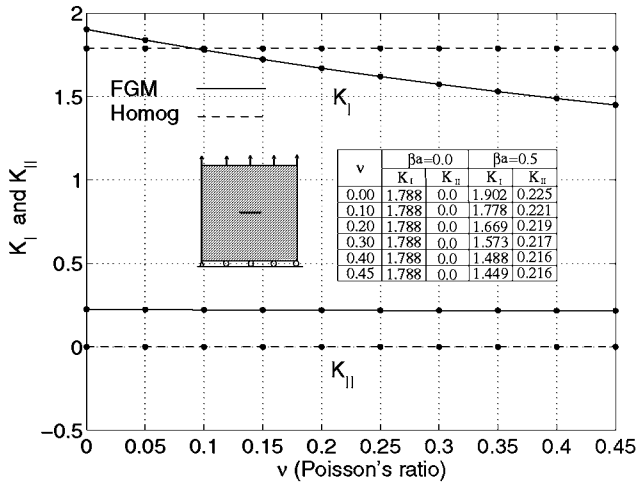

ν	βa=0.0		βa=0.5	
	K_I	K_{II}	K_I	K_{II}
0.00	1.788	0.0	1.902	0.225
0.10	1.788	0.0	1.778	0.221
0.20	1.788	0.0	1.669	0.219
0.30	1.788	0.0	1.573	0.217
0.40	1.788	0.0	1.488	0.216
0.45	1.788	0.0	1.449	0.216

Fig. 8. Example 2: SIFs obtained by the non-equilibrium formulation considering $\beta a = 0.0$ and $\beta a = 0.5$, and various constant Poisson's ratios ($\theta = 0°$). Ratio of plate size to crack length is 10.

Poisson's ratio effect is investigated for a fixed ratio $a/W = 0.1$, which approximates a crack in an infinite homogeneous domain. Fig. 8 shows the FEM results for SIFs obtained by the non-equilibrium formulation of the interaction integral method considering $\beta a = 0$ and $\beta a = 0.5$, and various constant Poisson's ratios for $\theta = 0°$. For homogeneous materials ($\beta a = 0.0$), SIFs are not affected by Poisson's ratio, however, for FGMs ($\beta a = 0.5$), Poisson's ratio has much influence on mode I SIF, i.e. K_I. Fig. 9 shows phase angle $\psi = \tan^{-1}(K_{II}/K_I)$ obtained by the non-equilibrium formulation considering βa = (0.0 to 0.5) and various constant Poisson's ratios for $\theta = 0°$. Notice that Poisson's ratio influences the phase angle for FGMs. For the homogeneous case, the phase angle $\psi = \tan^{-1}(K_{II}/K_I)$=0.0 because $K_{II} = 0$. However, in the FGM case considering constant Poisson's ratio, as the dimensionless nonhomogeneity parameter βa increases, the phase angle increases with increasing ratio K_{II}/K_I. Fig. 10 shows the FEM results for T-stress obtained by the non-equilibrium formulation considering $\beta a = 0$ and $\beta a = 0.5$, and various constant Poisson's ratios for $\theta = 0°$. Notice that, for homogeneous materials ($\beta a = 0.0$), T-stress is not affected by Poisson's ratio, however, for FGMs ($\beta a = 0.5$), it increases as Poisson's ratio increases. Figs. 11 and 12 show SIFs and T-stress, respectively, calculated by the non-equilibrium formulation for the right crack tip of a center crack with $\theta = 0°$ using four contours for EDI computations as shown in Fig. 7(d). The non-equilibrium formulation is used both considering and neglecting the non-equilibrium term (see Eq.(17)). Notice that the converged solution for SIFs and T-stress is obtained when including the non-equilibrium, however, such behavior is not observed when neglecting the non-equilibrium term. Thus Figs. 11 and 12 show that the non-equilibrium term must be considered in the M-integral formulation, especially when finite domains are considered around the crack tip.

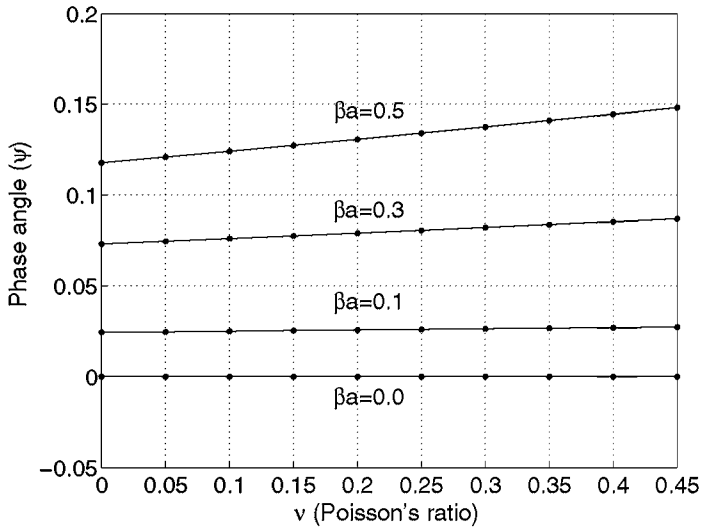

Fig. 9. Example 2: phase angle $\psi = \tan^{-1}(K_{II}/K_I)$ for various constant Poisson's ratios ($\theta = 0°$).

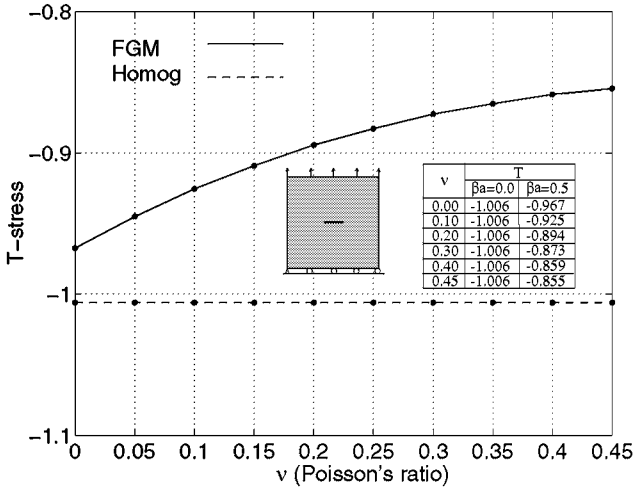

ν	T	
	βa=0.0	βa=0.5
0.00	-1.006	-0.967
0.10	-1.006	-0.925
0.20	-1.006	-0.894
0.30	-1.006	-0.873
0.40	-1.006	-0.859
0.45	-1.006	-0.855

Fig. 10. Example 2: T-stress obtained by the non-equilibrium formulation considering $\beta a = 0.0$ and $\beta a = 0.5$, and various constant Poisson's ratios. Ratio of plate size to crack length is 10.

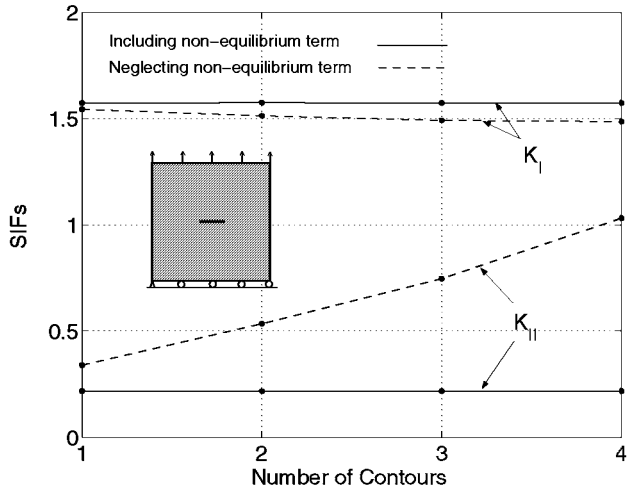

Fig. 11. Example 2: comparison of SIFs (K_I and K_{II}) obtained by the non-equilibrium formulation using four contours for the right crack tip of a center crack ($\theta = 0°$) (see Figure 7(d)). The non-equilibrium formulation is used both considering and neglecting the non-equilibrium term (see Eq.(17)).

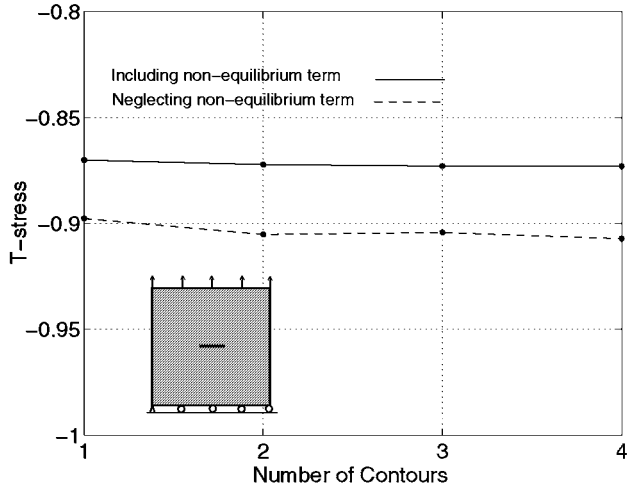

Fig. 12. Example 2: comparison of T-stress obtained by the non-equilibrium formulation using four contours for the right crack tip of a center crack ($\theta = 0°$) (see Figure 7(d)). The non-equilibrium formulation is used both considering and neglecting the non-equilibrium term (see Eq.(17)).

Table 2. Example 2: SIFs and T-stresses obtained by the non-equilibrium formulation considering $\beta a = 0.5$ and various sets of linearly varying Poisson's ratio for ($\theta = 0°$). The range of $\nu(X_2)$ is from the bottom to the top.

Case	$\nu(X_2)$ range	K_I	K_{II}	T
1	0.20–0.1	1.682	0.219	-0.910
2	0.30–0.1	1.596	0.217	-0.899
3	0.40–0.1	1.518	0.215	-0.893
4	0.45–0.1	1.482	0.215	-0.892

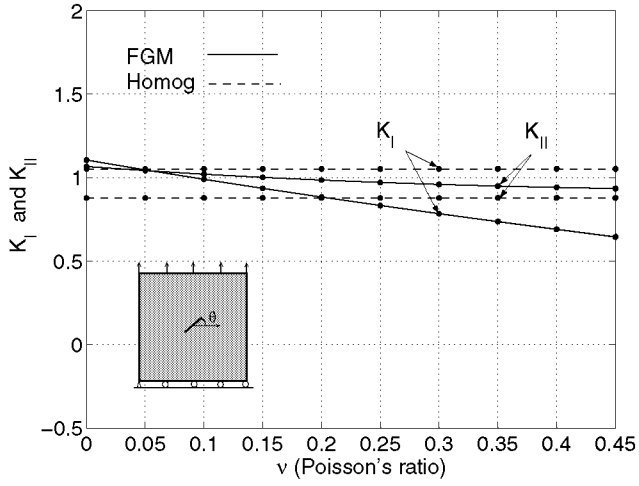

Fig. 13. Example 2: SIFs obtained by the non-equilibrium formulation considering $\beta a = 0.0$ and $\beta a = 0.5$, and various constant Poisson's ratios ($\theta = 40°$).

Table 2 shows FEM results for SIFs and T-stresses obtained by the non-equilibrium formulation considering four sets of linearly varying Poisson's ratio for $\theta = 0°$. Notice that linearly varying Poisson's ratio has influence on mode I SIF, however, its influence on T-stress is somewhat negligible.

The Poisson's ratio effect is also investigated for a fixed $a/W = 0.1$ and $\theta = 40°$. Figs. 13 and 14 show the FEM results for SIFs and T-stress, respectively, obtained by the non-equilibrium formulation considering $\beta a = 0.0$ and $\beta a = 0.5$, and various constant Poisson's ratios. Notice that, for homogeneous materials ($\beta a = 0.0$), SIFs and T-stress are not affected by Poisson's ratio, however, for FGMs ($\beta a = 0.5$), Poisson's ratio has much influence on mixed-mode SIFs (K_I and K_{II}), and its effect on the variation of T-stress is less significant. To allow comparison of results, Figs. 8 and 13 are plotted on the same scale.

The plate-size effect is investigated for different ratios $W/a =$ (2 to 12.5) considering $\theta = 0°$ and various Poisson's ratio variation (i.e. constant and linear). Figs. 15, 16, and 17 show the FEM results for SIFs obtained by the non-equilibrium formulation for different

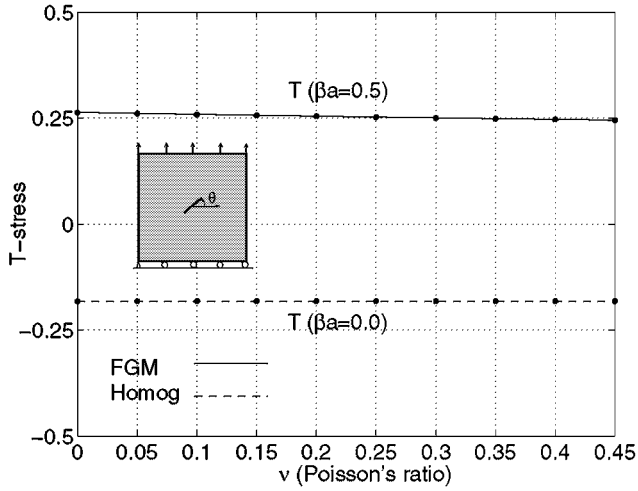

Fig. 14. Example 2: T-stress obtained by the non-equilibrium formulation considering $\beta a = 0.0$ and $\beta a = 0.5$, and various constant Poisson's ratios ($\theta = 40°$).

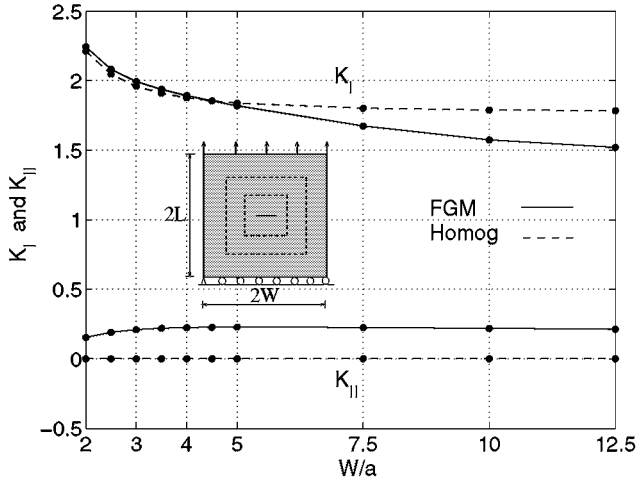

Fig. 15. Example 2: SIFs obtained by the non-equilibrium formulation considering $\beta a = 0.0$ (homogeneous material) and $\beta a = 0.5$ (FGM), and $\nu = 0.30$ for various plate sizes.

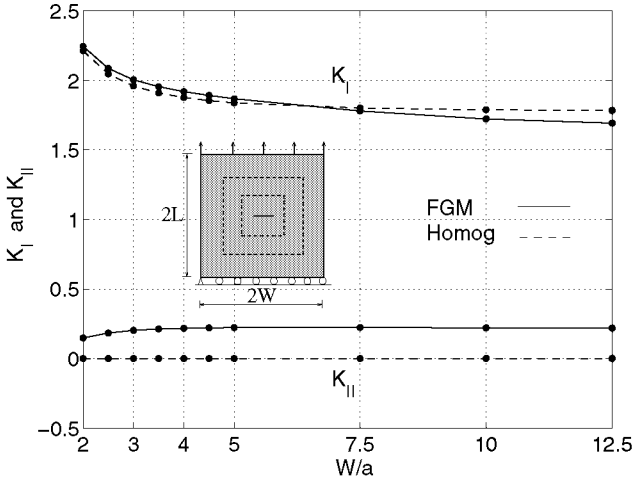

Fig. 16. Example 2: SIFs obtained by the non-equilibrium formulation considering $\beta a = 0.0$ (homogeneous material) and $\beta a = 0.5$ (FGM), and $\nu = 0.15$ for various plate sizes.

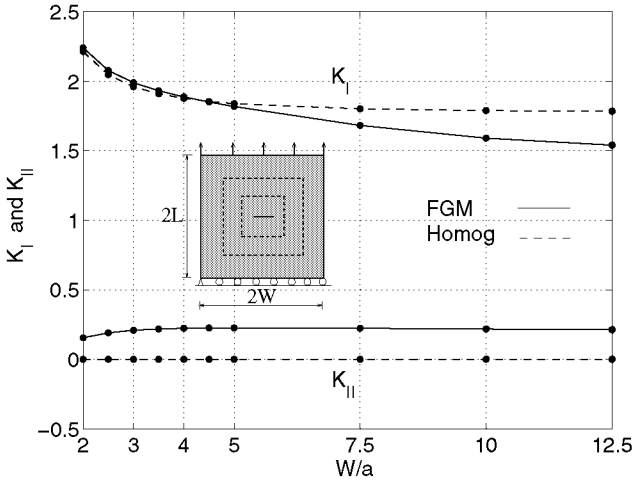

Fig. 17. Example 2: SIFs obtained by the non-equilibrium formulation considering $\beta a = 0.0$ (homogeneous material) and $\beta a = 0.5$ (FGM) for various plate sizes. The Poisson's ratio is assumed constant for the homogeneous material case ($\nu = 0.225$) and it varies linearly for the FGM case ($\nu(X_2) = 0.3$ to 0.15).

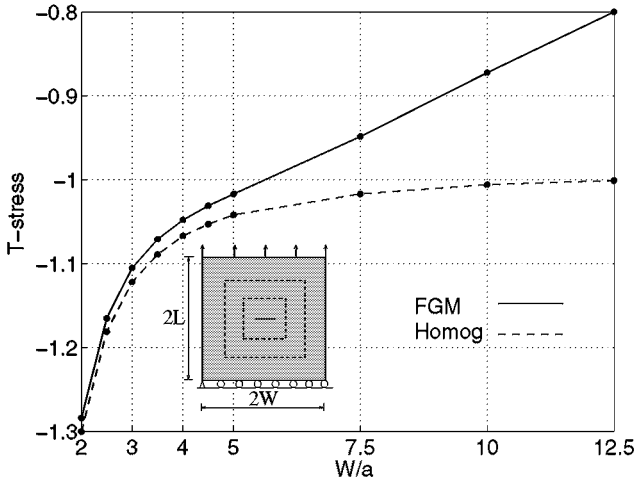

Fig. 18. Example 2: T-stress obtained by the non-equilibrium formulation considering $\beta a = 0.0$ (homogeneous material) and $\beta a = 0.5$ (FGM), and $\nu = 0.3$ for various plate sizes.

ratios a/W considering $\nu = 0.3$, $\nu = 0.15$, and linearly varying Poisson's ratios (an averaged Poisson's ratio $\nu = 0.225$ is used for the homogeneous case), respectively. Notice that, for each plate size, the Poisson's ratio has no influence on SIFs for homogeneous case, while it has significant influence on SIFs for FGM case. For instance, for plate size $2W = 2L = 15$ and $W/a = 7.5$, we have K_I=1.801 for all sets of Poisson's ratio considered for the homogeneous case, but, for the FGM case, K_I=1.673, 1.780, and 1.682 for $\nu = 0.3$, $\nu = 0.15$, and linearly varying Poisson's ratios ($\nu(X_2) = 0.3 \rightarrow 0.15$), respectively. Moreover, mixed-mode SIFs are not sensitive to plate size of 20 × 20 or larger for the homogeneous case, while the Mode I SIF is dependent on the plate size for the FGM case. The change of mode I SIF K_I is more significant than the mode II SIF K_{II}, especially as the plate size decreases.

Figs. 18, 19, and 20 show the FEM results for T-stress obtained by the non-equilibrium formulation for different ratios a/W considering $\nu = 0.3$, $\nu = 0.15$, and linearly varying Poisson's ratios (an averaged Poisson's ratio for the homogeneous case), respectively. The effect of the Poisson's ratio on T-stress become significant as the plate size increases. For each plate size, Poisson's ratio has no influence on T-stress for homogeneous case, while it has an influence on T-stress for FGM case. For instance, for plate size $2W = 2L = 15$ and $W/a = 7.5$, we have T=-1.017 for all sets of Poisson's ratio considered for the homogeneous case, but, for the FGM case, T=-0.9486, -0.9572, and -0.9586 for $\nu = 0.3$, $\nu = 0.15$, and linearly varying Poisson's ratios ($\nu(X_2) = 0.3 \rightarrow 0.15$), respectively. Moreover, for homogeneous materials, the T-stress shows little variation as the plate size increases, however, for the FGM case, the T-stress increases as the plate size increases.

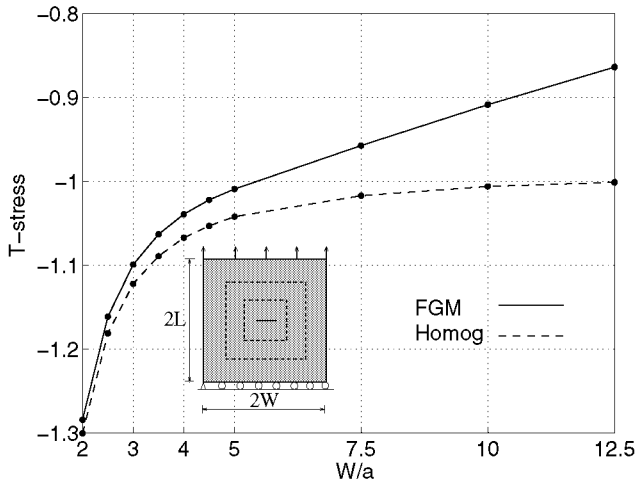

Fig. 19. Example 2: T-stress obtained by the non-equilibrium formulation considering $\beta a = 0.0$ (homogeneous material) and $\beta a = 0.5$ (FGM), and $\nu = 0.15$ for various plate sizes.

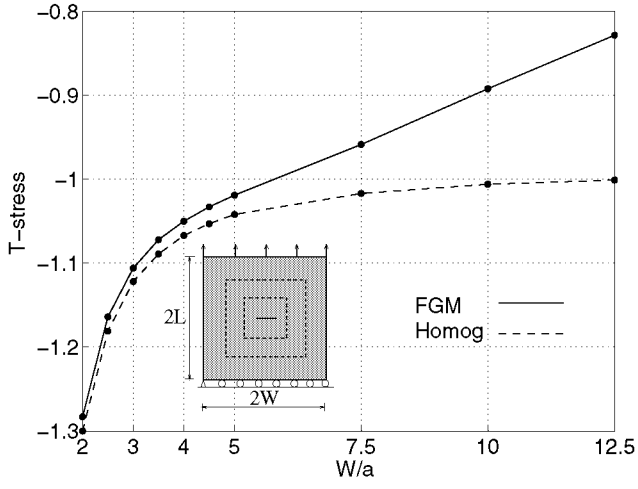

Fig. 20. Example 2: T-stress obtained by the non-equilibrium formulation considering $\beta a = 0.0$ (homogeneous material) and $\beta a = 0.5$ (FGM) for various plate sizes. The Poisson's ratio is assumed constant for the homogeneous material case ($\nu = 0.225$) and it varies linearly for the FGM case ($\nu(X_2) = 0.3$ to 0.15).

8.3. Center crack in a composite plate

Fig. 21(a) shows a center crack of length "$2a$" in a plate with hyperbolic-tangent variation of Young's modulus, and Fig. 21(b) shows the complete mesh discretization, and Fig. 21(c) shows mesh detail using 12 sectors (S12) and 4 rings (R4) around the crack tips. The applied load corresponds to $\sigma_{22}(X_1, 2.5) = \sigma = 1.0$. The displacement boundary conditions (BCs) are prescribed such that $u_1 = 0$ and $u_2 = 0$ at the left-corner node of the bottom edge and $u_2 = 0$ for the nodes of the bottom edge. The mesh discretization consists of 441 Q8, 122 T6, and 24 T6qp elements, with a total of 587 elements and 1712 nodes.

Young's modulus is a hyperbolic-tangent function with respect to the global X_2 Cartesian coordinate (see Fig. 22), while Poisson's ratio is constant. The following data were used for the FEM analysis:

$$\begin{gathered}\text{plane stress}, 2 \times 2 \text{ Gauss quadrature},\\ a/W = 0.2, L/W = 1.0,\\ E(X_2) = (E^+ + E^-)/2 + \tanh(\beta X_2)(E^+ - E^-)/2,\\ \beta a = (0.0, 2.5),\ (E^-, E^+) = (1.00, 5.00),\\ \nu = (0.0 \text{ to } 0.45)\end{gathered} \tag{43}$$

Fig. 23 shows the FEM results for SIFs obtained by the non-equilibrium formulation of the interaction integral method considering $\beta a = 0$ and $\beta a = 2.5$, and various constant Poisson's ratios. Notice that, for homogeneous materials ($\beta a = 0.0$), SIFs are not affected by Poisson's ratio, however, for FGMs ($\beta a = 2.5$), Poisson's ratio has much influence on mixed-mode SIFs, i.e. K_I and K_{II}. Comparison between Fig. 8 (exponential variation) and Fig. 23 (hyperbolic-tangent variation) indicates that as the Poisson's ratio increases K_I decreases for the former case, but K_I increases and decreases for the latter case.

Fig. 24 shows the FEM results for T-stress obtained by the non-equilibrium formulation considering $\beta a = 0$ and $\beta a = 2.5$, and various constant Poisson's ratios. Notice that, for homogeneous materials ($\beta a = 0.0$), T-stress is not affected by Poisson's ratio, however, for FGMs ($\beta a = 0.5$), it decreases in the form of a half-wave as Poisson's ratio increases (0.0 to 0.45). Comparison between Fig. 10 (exponential variation) and Fig. 24 (hyperbolic-tangent variation) indicates that as the Poisson's ratio increases T-stress increases for the former case, but it decreases for the latter case.

9. Conclusions

This paper investigates the effect of Poisson's ratio on both SIFs and T-stress in two-dimensional (2D) elastic FGMs using the non-equilibrium formulation of the interaction integral method in conjunction with the FEM. When tension load is applied in the direction parallel to material gradation, the more compliant part of the material may show

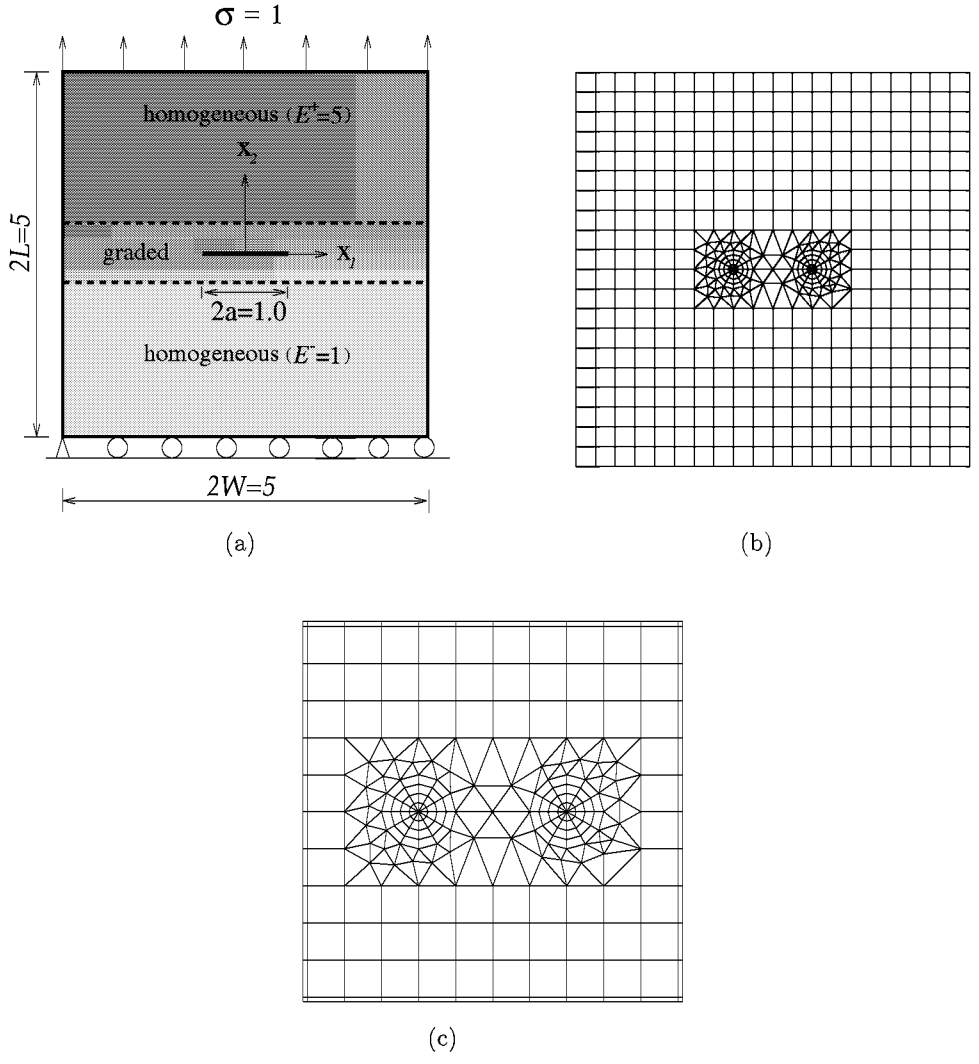

Fig. 21. Example 3: composite plate with a center crack. (a) geometry and BCs; (b) complete finite element mesh; (c) mesh detail using 12 sectors (S12) and 4 rings (R4) of elements around the crack tips.

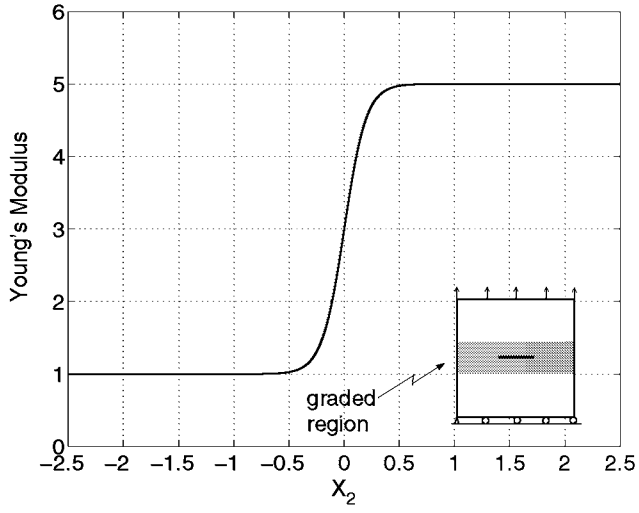

Fig. 22. Example 3: variation of Young's modulus (E) with position (X_2).

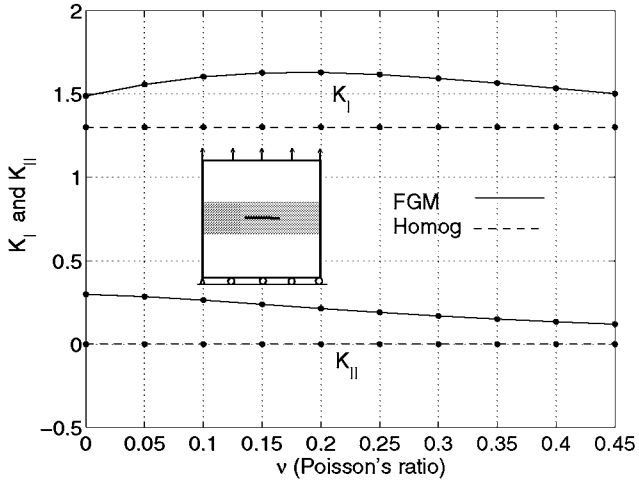

Fig. 23. Example 3: SIFs obtained by the non-equilibrium formulation considering $\beta a = 0.0$ and $\beta a = 2.5$, and various constant Poisson's ratios.

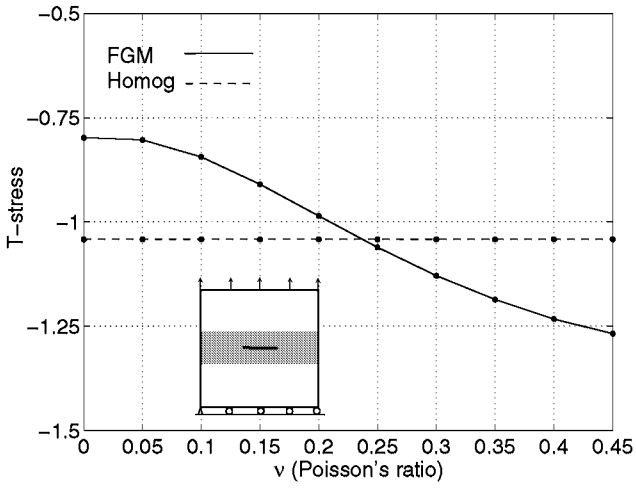

Fig. 24. Example 3: T-stress obtained by the non-equilibrium formulation considering $\beta a = 0.0$ and $\beta a = 2.5$, and various constant Poisson's ratios.

more contraction than the stiffer part. This behavior affects the near crack-tip fields characterized by SIFs and T-stress. The numerical examples show that Poisson's ratio has a significant influence on both SIFs and T-stress for FGMs. Its effect on these parameters become significant as material nonhomogeneity increases. The type of material gradation (e.g. exponential or hyperbolic-tangent function) also has a significant influence on such parameters. Moreover, for the FGM case, the nonhomogeneity parameter introduces a geometrical length scale, e.g. $1/\beta$ in Eq.(41), and the plate size interplays with such length scale. For FGMs, the Poisson's ratio influences the fracture parameters as the plate size changes, however, as expected, it has no influence for homogeneous materials (see Figs. 15 to 20).

This paper provides useful information on the effect of Poisson's ratio on fracture parameters in FGMs. It also emphasizes that more attention needs to be paid to Poisson's ratio effect, especially when load direction becomes parallel to the direction of material gradation.

Acknowledgements

We gratefully acknowledge the support from NASA-Ames, Engineering for Complex Systems Program, and the NASA-Ames Chief Engineer (Dr. Tina Panontin) through grant NAG 2-1424. We also acknowledge additional support from the National Science Foundation (NSF) under grant CMS-0115954 (Mechanics & Materials Program). Any opinions expressed herein are those of the writers and do not necessarily reflect the views of the sponsors.

References

1. J. W. Eischen. Fracture of non-homogeneous materials. *International Journal of Fracture*, 34(1):3–22, 1987.
2. J.-H. Kim and G. H. Paulino. Finite element evaluation of mixed-mode stress intensity factors in functionally graded materials. *International Journal for Numerical Methods in Engineering*, 53(8):1903–1935, 2002.
3. P. R. Marur and H. V. Tippur. Numerical analysis of crack-tip fields in functionally graded materials with a crack normal to the elastic gradient. *International Journal of Solids and Structures*, 37(38):5353–5370, 2000.
4. J. Dolbow and M. Gosz. On the computation of mixed-mode stress intensity factors in functionally graded materials. *International Journal of Solids and Structures*, 39(9):2557–2574, 2002.
5. B. N. Rao and S. Rahman. Mesh-free analysis of cracks in isotropic functionally graded materials. *Engineering Fracture Mechanics*, 70(1):1–27, 2003.
6. J.-H. Kim and G. H. Paulino. An accurate scheme for mixed-mode fracture analysis of functionally graded materials using the interaction integral and micromechanics models. *International Journal for Numerical Methods in Engineering*, 58(10):1457–1497, 2003.
7. J.-H. Kim and G. H. Paulino. Consistent formulations of the interaction integral method for fracture of functionally graded materials. *Journal of Applied Mechanics, Transactions ASME*, 72(3):351–364, 2005.
8. T. L. Becker Jr., R. M. Cannon, and R. O. Ritchie. Finite crack kinking and T-stresses in functionally graded materials. *International Journal of Solids and Structures*, 38(32-33):5545–5563, 2001.
9. J.-H. Kim and G. H. Paulino. T-stress, mixed-mode stress intensity factors, and crack initiation angles in functionally graded materials: A unified approach using the interaction integral method. *Computer Methods in Applied Mechanics and Engineering*, 192(11-12):1463–1494, 2003.
10. G. H. Paulino and J.-H. Kim. A new approach to compute T-stress in functionally graded materials using the interaction integral method. *Engineering Fracture Mechanics*, 71(13–14):1907–1950, 2004.
11. J. K. Knowles and E. Sternberg. On a class of conservation laws in linearized and finite elastostatics. *Archive for Rational Mechanics and Analysis*, 44(2):187–211, 1972.
12. B. Budiansky and J. R. Rice. Conservation laws and energy-release rates. *Journal of Applied Mechanics, Transactions ASME*, 40(1):201–203, 1973.
13. J. H. Chang and A. J. Chien. Evaluation of M-integral for anisotropic elastic media with multiple defects. *International Journal of Fracture*, 114(3):267–289, 2002.
14. M. F. Kanninen and C. H. Popelar. *Advanced Fracture Mechanics*. Oxford University Press, New York, 1985.

15. J. F. Yau, S. S. Wang, and H. T. Corten. A mixed-mode crack analysis of isotropic solids using conservation laws of elasticity. *Journal of Applied Mechanics, Transactions ASME*, 47(2):335–341, 1980.
16. M. L. Williams. On the stress distribution at the base of a stationary crack. *Journal of Applied Mechanics, Transactions ASME*, 24(1):109–114, 1957.
17. P. Gu, M. Dao, and R. J. Asaro. A simplified method for calculating the crack-tip field of functionally graded materials using the domain integral. *Journal of Applied Mechanics, Transactions ASME*, 34(1):1–17, 1997.
18. G. Anlas, M. H. Santare, and J. Lambros. Numerical calculation of stress intensity factors in functionally graded materials. *International Journal of Fracture*, 104(2):131–143, 2000.
19. G. Bao and H. Cai. Delamination cracking in functionally graded coating/metal subst rate systems. *Acta Mechanica*, 45(3):1055–1066, 1997.
20. G. Bao and L. Wang. Multiple cracking in functionally graded ceramic/metal coatings. *International Journal of Solids and Structures*, 32(19):2853–2871, 1995.
21. Z.-H. Jin and N. Noda. Crack-tip singular fields in nonhomogeneous materials. *Journal of Applied Mechanics, Transactions ASME*, 61(3):738–740, 1994.
22. J. Eftis, N. Subramonian, and H. Liebowitz. Crack border stress and displacement equations revisited. *Engineering Fracture Mechanics*, 9(1):189–210, 1977.
23. S. P. Timoshenko and J. N. Goodier. *Theory of Elasticity, 3rd Edition.* McGraw-Hill, New York, 1987.
24. J. R. Rice. A path-independent integral and the approximate analysis of strain concentration by notches and cracks. *Journal of Applied Mechanics, Transactions ASME*, 35(2):379–386, 1968.
25. I. S. Raju and K. N. Shivakumar. An equivalent domain integral method in the two-dimensional analysis of mixed mode crack problems. *Engineering Fracture Mechanics*, 37(4):707–725, 1990.
26. J.-H. Kim and G. H. Paulino. Isoparametric graded finite elements for nonhomogeneous isotropic and orthotropic materials. *Journal of Applied Mechanics, Transactions ASME*, 69(4):502–514, 2002.
27. R. D. Cook, D. S. Malkus, M. E. Plesha, and R. J. Witt. *Concepts and applications of finite element analysis (4th edition).* John Wiley & Sons, Inc., New York, 2001.
28. P. A. Wawrzynek. Interactive finite element analysis of fracture processes: an integrated approach. *M.S. Thesis, Cornell University*, 1987.
29. P. A. Wawrzynek and A. R. Ingraffea. Discrete modeling of crack propagation: theoretical aspects and implementation issues in two and three dimensions. *Report 91-5, School of Civil Engineering and Environmental Engineering, Cornell University*, 1991.

30. M. H. Santare and J. Lambros. Use of graded finite elements to model the behavior of nonhomogeneous materials. *Journal of Applied Mechanics, Transactions ASME*, 67(4):819–822, 2000.
31. F. Erdogan. Fracture mechanics of functionally graded materials. *Composites Engineering*, 5(7):753–770, 1995.
32. F. Delale and F. Erdogan. The crack problem for a nonhomogeneous plane. *Journal of Applied Mechanics, Transactions ASME*, 50(3):609–614, 1983.
33. F. Erdogan and B. H. Wu. The surface crack problem for a plate with functionally graded properties. *Journal of Applied Mechanics, Transactions ASME*, 64(3):449–456, 1997.
34. Y.-S. Chan, G. H. Paulino, and A. C. Fannjiang. The crack problem for nonhomogeneous materials under antiplane shear loading – A displacement based formulation. *International Journal of Solids and Structures*, 38(17):2989–3005, 2001.
35. F. Delale and F. Erdogan. On the mechanical modeling of an interfacial region in bonded half-planes. *Journal of Applied Mechanics, Transactions ASME*, 55(2):317–324, 1988.
36. N. I. Shbeeb, W. K. Binienda, and K. L. Kreider. Analysis of the driving forces for multiple cracks in an infinite nonhomogeneous plate, Part I: Theoretical analysis. *Journal of Applied Mechanics, Transactions ASME*, 66(2):492–500, 1999.
37. N. I. Shbeeb, W. K. Binienda, and K. L. Kreider. Analysis of the driving forces for multiple cracks in an infinite nonhomogeneous plate, Part II: Numerical solutions. *Journal of Applied Mechanics, Transactions ASME*, 66(2):501–506, 1999.
38. T. Honein and G. Herrmann. Conservation laws in nonhomogeneous plane elastostatics. *Journal of the Mechanics and Physics of Solids*, 45(5):789–805, 1997.
39. N. Konda and F. Erdogan. The mixed mode crack problem in a nonhomogeneous elastic medium. *Engineering Fracture Mechanics*, 47(4):533–545, 1994.
40. G. H. Paulino and Z. Dong. A novel application of the singular integral equation approach to evaluate T-stress in functionally graded materials (in preparation).